

PAPER View Article Online
View Journal | View Issue



Cite this: *Phys. Chem. Chem. Phys.*, 2021, **23**, 4030

# Enhanced performance of Mo<sub>2</sub>P monolayer as lithium-ion battery anode materials by carbon and nitrogen doping: a first principles study†

Xinghui Liu, ab Shiru Lin, bc Jian Gao, Hu Shi, be Seong-Gon Kim, Zhongfang Chen b\* and Hyoyoung Lee b\* Abb

By means of density functional theory (DFT) computations, we explored the potential of carbon- and nitrogen-doped  $Mo_2P$  (CMP and NMP) layered materials as the representative of transition metal phosphides (TMPs) for the development of lithium-ion battery (LIB) anode materials, paying special attention to the synergistic effects of the dopants. Both CMP and NMP have exceptional stabilities and excellent electronic conductivity, and a high theoretical maximum storage capacity of  $\sim 486$  mA h g $^{-1}$ . Li-ion diffusion barriers on the two-dimensional (2D) CMP and NMP surfaces are extremely low ( $\sim 0.036$  eV), and it is expected that on these 2D layers Li can diffuse  $10^4$  times faster than that on  $MoS_2$  and graphene at room temperature, and both monolayers have relatively low average open-circuit voltage (0.38 and 0.4 eV). All these exceptional properties make CMP and NMP monolayers as promising candidates for high-performance LIB anode materials, which also demonstrates that simple doping is an effective strategy to enhance the performance of anode materials in rechargeable batteries.

Received 12th December 2020, Accepted 28th January 2021

DOI: 10.1039/d0cp06428a

rsc.li/pccp

#### 1. Introduction

Lithium-ion batteries (LIBs) are the most widely used rechargeable batteries and hold great promise for even larger scale applications in the very near future due to their exceptional characteristics, such as excellent energy efficiency, high-energy-density, long-life cycle, and being environmentally benign.<sup>1–4</sup> To further improve the performance of LIBs, it is urgent to develop advanced electrode materials that can provide the high-density energy storage and ultra-fast charge rate.<sup>5</sup>

Two-dimensional (2D) materials are expected to be critical components for not only electronic devices, <sup>6</sup> but also for energy

storage applications such as supercapacitors<sup>7</sup> and batteries,<sup>8</sup>

because of their extraordinary structural, electronic, and mechanical properties. Typically, graphite is used as the anode

in commercial LIBs due to its excellent cycling stability and low

Bulk transition metal phosphides (BTMPs), firstly systematically described by Schnering and Hönle in 1988,<sup>23</sup> are a class of emerging materials in energy storage and conversion.<sup>24,25</sup> Alloying phosphorus and metals, BTMPs are categorized as three types: MP<sub>2</sub> (phosphorus-rich compounds with semiconductor properties, considerably less stable than the metal-rich compounds), MP (metallic), and M<sub>2</sub>P (metal-rich compounds with metallic properties, good conductors of heat and electricity with high chemical and thermal stability).<sup>26,27</sup> In 2002, Nazar *et al.* experimentally observed reversible Li uptake by a BTMP electrode, CoP<sub>3</sub>, at a low potential,<sup>28</sup> which gained much attention due to its high gravimetric capacity and lower polarization than sulfides, fluorides, and oxides.<sup>29–32</sup>

cost. Still, the relatively low capacity (372 mA h g<sup>-1</sup>) and poor rate performance limit its further applications.<sup>8</sup> In this regard, 2D materials are promising candidates as next-generation LIB anode materials to achieve high surface areas, high-energy storage density, low ion diffusion barrier, and other intriguing features.<sup>8-11</sup> Numerous 2D materials, such as graphene, s,12-14 transition-metal dichalcogenides (TMD), s,13,15-17 transition metal oxides (TMOs), stransition metal carbides and nitrides (MXenes), solvential electrode materials for LIBs.

<sup>&</sup>lt;sup>a</sup> Center for Integrated Nanostructure Physics (CINAP), Institute of Basic Science (IBS), 2066 Seoburo, Jangan-Gu, Suwon 16419, Republic of Korea

<sup>&</sup>lt;sup>b</sup> Department of Chemistry, Sungkyunkwan University (SKKU), 2066 Seoburo, Jangan-Gu, Suwon 16419, Republic of Korea. E-mail: hyoyoung@skku.edu

<sup>&</sup>lt;sup>c</sup> Department of Chemistry, University of Puerto Rico, Rio Piedras Campus, San Juan, USA. E-mail: zhongfangchen@gmail.com

<sup>&</sup>lt;sup>d</sup> State Key Laboratory of Organic-Inorganic Composites, Beijing University of Chemical Technology, Beijing 100029, China

<sup>&</sup>lt;sup>e</sup> School of Chemistry and Chemical Engineering, Shanxi University, Taiyuan, People's Republic of China

<sup>&</sup>lt;sup>f</sup> Department of Physics and Astronomy, Mississippi State University, Mississippi State, MS 39762, USA

g Department of Biophysics, Sungkyunkwan University (SKKU), 2066 Seoburo, Jangan-Gu, Suwon 16419, Republic of Korea

 $<sup>\</sup>dagger$  Electronic supplementary information (ESI) available. See DOI: 10.1039/d0cp06428a

Paper

Very recently, great progress has been achieved on 2D M<sub>2</sub>Ps.<sup>33</sup> Theoretically, W<sub>2</sub>P, Sr<sub>2</sub>P, and Mo<sub>2</sub>P were confirmed to be dynamically and thermodynamically stable.33-35 Experimentally, Yang et al. demonstrated a topochemical strategy to prepare Co<sub>2</sub>P and Fe<sub>2</sub>P using phosphorene as the P source.<sup>36</sup> Among these 2D M<sub>2</sub>Ps, Mo<sub>2</sub>P caught our great attention, since its metallicity, high tensile strength and elastic modulus, low Li diffusion energy barrier (50 meV), and low open-circuit voltage (0.88-1.06 V) endow 2D Mo<sub>2</sub>P as promising LIB anode materials.37 However, the Li storage capacity in 2D Mo<sub>2</sub>P  $(240 \text{ mA h g}^{-1})$  is even lower than graphite.<sup>8,37</sup> Thus, it is desirable to find a good strategy to improve its Li storage capacity while keeping or even lower the Li diffusion energy barriers.

Different strategies, such as chemical functionalization<sup>38</sup> mechanical engineerings, 39,40 and heteroatom doping, 41-47 have been utilized to tune the properties of 2D materials. Among these strategies, doping heteroatoms (e.g., carbon, nitrogen, boron, etc.) into 2D materials has been proven as an effective method to increase storage capacity, surface wettability, and conductivity of LIB anode materials. 41-47 For example, Reddy et al. successfully fabricated nitrogen-doped graphene films with a high percentage of pyridinic N atoms and achieved much enhanced lithium-ion storage.43

Herein, we theoretically investigated the geometric and electronic properties, the stability, and electrochemical performance of carbon- and nitrogen-doped 2D Mo<sub>2</sub>P materials, namely CMP and NMP, paying special attention to the doping effects of heteroatoms, by systematic density functional theory (DFT) computations and ab initio molecular dynamics simulations (AIMD) simulations. Our computations showed that CMP and NMP are promising high-performance LIB anode materials, and once again demonstrated that simple doping is an effective strategy to enhance the performance of anode materials in rechargeable batteries.

## 2. Computational methods

All our DFT calculations and ab initio molecular dynamic simulations were carried out by using Vienna Ab initio Simulation Package (VASP). <sup>48–50</sup> The projector-augmented wave (PAW) method was employed to describe the ion-electron interaction. 51,52 The exchange-correlation function was depicted by the generalized gradient approximation in the form of Perdew-Burke-Ernzerhof (GGA-PBE) functional.<sup>53</sup> The electronic wave functions were expanded using a plane-wave basis with 500 eV cutoff energy. Monkhorst-Pack k points mesh sizes of 7  $\times$  7  $\times$  1 and 13  $\times$  13  $\times$  1 were used for geometric optimizations and self-consistent total energy calculations, respectively.<sup>54</sup> All the structures were optimized with the convergence criteria of 10<sup>-4</sup> eV Å<sup>-1</sup> in force and 10<sup>-6</sup> eV per atom in energy. To assess the kinetic stability, phonon dispersion of the CMP(NMP) monolayer was computed using the finite displacement method as implanted in the PHONOPY program.<sup>55</sup> A 15 Å vacuum space in the z-direction was applied to avoid interactions between adjacent periodic images.

To confirm the thermal stability of CMP and NMP, the AIMD simulations were carried out using  $4 \times 4$  super-cells in the NVT ensemble with the Nosé thermostat method. Each simulation lasted 20 ps with a time step of 2.0 fs, and the k-point mesh size was set as  $3 \times 3 \times 1.56$  Li diffusion coefficients were calculated from the mean square displacements using  $2 \times 2$ super-cells in the NVT ensemble with the Nosé thermostat method. Each simulation lasted 40 ps with a time step of 2.0 fs, and the gamma point was used for all temperature simulations. The long-range dispersion correction scheme of zero dampings developed by Grimme, i.e. the DFT-D3 method, was employed to describe the van der Waals interactions of adsorption modes.<sup>57</sup> The climbing-image nudged elastic band (CI-NEB) methods were used to evaluate Li-ion diffusion pathways and the diffusion barrier.  $^{58,59}$  The energy barrier  $(E_a)$  is defined as  $E_a = E_{TS} - E_{IS}$ , where  $E_{TS}$  and  $E_{IS}$  represent the energies of the transition state and the initial state, respectively.

The lithiation/delithiation of C(N)MP process on the anode can be summarized as

$$Li_xC(N)MP \xrightarrow{charge/discharge} xLi^+ + C(N)MP + xe^-$$

To study the Li atom adsorption on the C(N)MP monolayer, we investigated different adsorption sites (S1, S2, and S3) on  $2 \times 2$  super-cell models (Fig. 1). The most favorable adsorption configurations were identified by comparing their Li atom adsorption energies  $(E_{ad})$ , defined as

$$E_{\rm ad} = \frac{E_{\rm Li_xC(N)MP} - xE_{\rm Li} - E_{\rm C(N)MP}}{x} \tag{2}$$

where  $E_{\mathrm{Li}_{r}\mathrm{C}(\mathrm{N})\mathrm{MP}}$  and  $E_{\mathrm{C}(\mathrm{N})\mathrm{MP}}$  are the total energies of the C(N)MP monolayer with and without Li atom adsorbed,

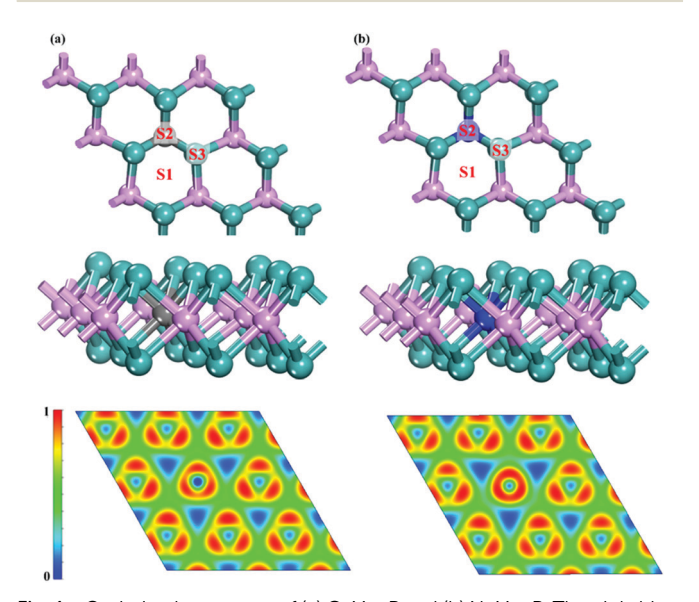


Fig. 1 Optimized structures of (a) C-Mo<sub>2</sub>P and (b) N-Mo<sub>2</sub>P. The pink, blue, grey, and dark-blue balls represent P, Mo, C, and N atoms, respectively. In the low panel are the contour plots of the electron localization function (ELF) map sliced in the direction of the monolayers.

**PCCP** Paper

respectively,  $E_{Li}$  is the total energy of metallic Li bulk, and x is the number of Li atoms adsorbed per formula unit.

The open-circuit voltage (OCV), the potential difference between the two terminals of the cell when disconnected from any circuit, is an important metric in determining the state of charge and state of health in LIBs. The average OCVs were obtained by averaging the values of the calculated voltage profile for different lithiation degrees. In principle, OCV should be calculated from the Nernst equation. However, the pressure term  $P\Delta V$  and the entropic term  $T\Delta S$  are negligible to the Gibbs free energy ( $\delta G = \Delta E + P\Delta V - T\Delta S$ ) at low temperature, thus only the energy term is used in voltage estimation. 12 Thus, the OCVs can be defined as

$$V_{\text{OCV}} = -\frac{\delta G}{xzF} \approx -\frac{E_{\text{Li}_{x_2}C(\text{N})\text{MP}} - E_{\text{Li}_{x_1}C(\text{N})\text{MP}} - (x_2 - x_1) \times E_{\text{Li}}}{(x_2 - x_1)F}$$
(3)

where  $E_{\text{Li}_{x_1}\text{C(N)MP}}$  and  $E_{\text{Li}_{x_1}\text{C(N)MP}}$  are the total energies of C(N)MP compounds with different lithiation degrees, respectively. z is equal to 1 for Li atom adsorption, and F is the Faraday constant.

To evaluate the Li diffusion on the 2D anode materials, we estimated the theoretical diffusivity D by the Arrhenius equation.

$$D \approx \exp\left(\frac{-E_{\rm a}}{k_{\rm B}T}\right) \tag{4}$$

where  $E_{\rm a}$ ,  $k_{\rm B}$  and T are the activation energy, the Boltzmann constant, and the temperature, respectively.

Specific storage capacity  $(C_{SP})$  is one of the most critical factors in the performance of electrode materials and can be evaluated by the equation

$$C_{\rm SP} = \frac{xzF}{M} \tag{5}$$

where M is the mass of the CMP(NMP) monolayer in g mol<sup>-1</sup>, xrepresents the number of electrons involved in the electrochemical process, z = 1 for Li atom adsorption, and F is the Faraday constant.

#### 3. Results and discussion

#### 3.1. Structure and stability properties

To construct the stable doped Mo<sub>2</sub>P monolayer, we need to wisely choose suitable dopants, for which we used a simple criterion based on the geometric fit. It is known that for a facecenter cubic, hexagonal close-packed or simple hexagonal in carbides, nitrides, and phosphides, the structure is generally stable when the ratio of  $R_{\rm X}/R_{\rm M}$  (radii of non-metal and metal elements) is between 0.41 and 0.59.27 Thus, carbon and nitrogen (atomic radii of 0.071 and 0.065 nm, respectively; in comparison, the radius of phosphorous is 0.109 nm) were of our choice, the resulting  $R_{\rm C}/R_{\rm Mo}$  (0.55) and  $R_{\rm N}/R_{\rm Mo}$  (0.50) values are in the favorable range (0.41-0.59) ( $R_{\text{Mo}} = 0.13 \text{ nm}$ ). It is expected that the C(N) atoms in the resulting CMP and NMP monolayers can be strongly bonded to Mo atoms, leading to a highly robust 2D materials with a high surface-to-volume ratio as the pristine 2D Mo<sub>2</sub>P monolayers.

As expected, our DFT computations confirmed the strong bonding between the C/N dopants and Mo atoms in CMP/NMP monolayers. The newly formed C-Mo bonds (2.13 Å) and N-Mo bonds (2.12 Å) are both shorter than the pristine P-Mo (2.35 Å) bonds (Fig. 1 and Fig. S1, ESI†), because of relatively smaller radii of C atoms and N atoms than the P atoms. Note that the C and N dopants have larger electronegativity values (Pauling scale: 2.55 and 3.04, respectively) than those of Mo elements (2.19 and 2.16, respectively), the electrons in both CMP and NMP layers are highly localized at heteroatoms C(N), as indicated in the electron localization function (ELF) plot (Fig. 1). Note that ELF<sup>60</sup> values of 1.0 and 0.5 indicate perfect electron localization and free electron gas (corresponding to metallic bond), respectively, while the value close to zero denotes a low electron density area. Typically, the large ELF number (>0.5)corresponds to a covalent bond or core electrons, while its value lower than 0.5 can be represented as the ionic bond. Here, the nearest-neighbor non-metal atoms suggest the significant P-Mo, C-Mo, and N-Mo covalent bonding. Besides, the charge delocalization is more concentrated around the Mo atoms as compared with the P atoms or dopant atoms. We further conducted the charge density difference to investigate the charge transfer of P-Mo, C-Mo, and N-Mo. The results showed (Fig. S2, ESI†) that the dopant (C and N) got more charge than P, and N got the highest charge from Mo among those elements, consistent with the electronegativity analysis. Furthermore, we applied Bader charge analysis<sup>61</sup> to discern the quantified electron transfer of the bonding characters in P-Mo, C-Mo, and N-Mo. As a result, it was found the P, C, and N got  $\sim 0.57 \sim 1.05$ , and 1.27 from Mo, respectively. Therefore, we can conclude that the C and N doping can modify the surface charge of Mo<sub>2</sub>P, indicating the more positive surface that beneficial for the intercalation of Li.

The structural stability of electrode materials is a dominant factor determining its long-time cycling charge/discharge characteristics of the lithium-ion battery. Thus, we systematically evaluate the stabilities of the CMP and NMP monolayers. First, we calculated the formation energy  $(H_f)$  by following the previous study, 62,63 defined by  $H_f = E_{\text{total}}[Mo_{18}P(9 - z)C_z] E_{\text{total}}[Mo_{18}P_9] + zE[P] - zE[C]$  for CMP and  $H_f = E_{\text{total}}[Mo_{18}P(9)]$ -z $N_z$ -z $E_{total}$  $Mo_{18}P_9$ +zE[P]-zE[N] for NMP. Where the first and second terms on the right side of the equation are the energies of doped and undoped Mo<sub>2</sub>P, respectively. The z is the number of the dopant atom. The E[P] and E[C](E[N]) are the chemical potentials atom for P and dopant of carbon (nitrogen), respectively, calculated using the most stable bulk phases. As a result, the obtained negative  $H_{\rm f}$  values (-5.99 eV and -8.78 eV for CMP and NMP, respectively) indicate that these two monolayers are thermodynamically favorable. Then, we calculated their phonon dispersion along with the highsymmetry  $\Gamma$ -M-K- $\Gamma$  direction and did not find any significant imaginary vibrational frequency (Fig. S3a and b, ESI†), which confirms the kinetic stability of these two doped monolayers. These results show that our predicted C(N)MP monolayer has a higher possibility to be synthesized under certain experimental conditions.

**PCCP** Paper

#### 3.2. Electronic structure properties

The electronic properties are important factors in determining the rate performance and battery cyclability of electrode materials. Therefore, we calculated electronic band structures and projected density of states (PDOS) of C(N)MP (Fig. 2 and Fig. S4, ESI†) at the PBE level of theory. The high PDOS peaks across the Fermi level reveal its intrinsic metallicity and high density of carriers, indicating excellent electronic conductivity. The atom-projected band structures of C(N)MP (Fig. S5, ESI†) show that the electronic band structure is dominated by the metal element (Mo), while the nonmetals elements (C, N, and P) make insignificant contributions to the electronic band structures near the Fermi level. This finding is inconsistent with the projected band structure of each atom (Fig. S6a and b, ESI†). As we expected, introducing C/N dopants into the Mo<sub>2</sub>P monolayer does not alter its intrinsic metallicity.

#### 3.3. Li atom adsorption and diffusion on the CMP/NMP monolayer

To evaluate the diffusion and storage properties of the lithiumion on the surface of the C(N)MP monolayer, we firstly investigated the preferred adsorption site of the lithium by using potential energy surfaces of a Li adatom.<sup>64</sup> As the result of potential energy surfaces of a Li adatom on CMP and NMP (Fig. S7a and b, ESI†), three possible adsorption sites strongly effect by the heteroatoms, marked as S1, S2, and S3 (Fig. 3). For pristine Mo<sub>2</sub>P, S1 has been reported as the most stable adsorption site with the largest binding energy compared to sites S2 and S3.37 For CMP, after full structure relaxation, we determined that the adsorption energies of S1, S2, and S3 are -0.63, -0.61, and -0.53 eV, respectively. Clearly, site S1 is the most stable adsorption site followed by sites S2 and S3 for CMP. However, as NMP is concerned, the adsorption energies of at sites S1, S2, and S3 are -0.60, -0.62, and -0.54 eV, respectively, indicating that the most favorable adsorption site is S2 for NMP, which is different from the case of CMP.

The Li diffusion barrier directly determines the chargedischarge rate capacity of LIBs, thus high Li mobility and low

diffusion barrier are desirable for promising anode electrode materials. With the aid of the nudged elastic band (NEB) method,58,59 we investigated the diffusion barriers of Li on C(N)MP between the nearest-neighboring low-energy adsorption sites along the three possible migration pathways. Specifically, the migration pathways of Li are selected between two adjacent lowest energy adsorption sites (S1 for CMP, and S2 for NMP). Accordingly, we examined the S1-S1, S1-S2-S1, and S1-S3-S1 pathways for CMP (Fig. 3a), while studied the S2-S2, S2-S1-S2, and S2-S3-S2 pathways for NMP (Fig. 3b), respectively. The schematic representations of the top view of the migration pathways and the diffusion barriers profiles are given in ESI† (Movies S1 to S3 for CMP and Movies S4 to S5).

For CMP, the diffusion barrier of the S1-S1, S1-S2-S1, and S1-S3-S1 pathways are 0.100 eV, 0.037 eV, and 0.037 eV (Fig. 3a), respectively. Consequently, the S1-S2(S3)-S1 pathways are kinetically more favorable than the S1-S1 pathway. For NMP, the diffusion barriers of Li migration on the surface NMP are different: the S2-S3-S2 pathway is undesirable because the energy barrier is high (0.078 eV) compared to the pristine Mo<sub>2</sub>P (0.051 eV<sup>37</sup>); both S2-S2 and S2-S1-S2 pathways exhibit the same diffusion barrier of 0.036 eV. The rather low Li diffusion barrier can be understood by the stabilization of the transition state, which facilitates the hybridization of Li orbital and the orbital of relatively electron-richer C/N atoms (in comparison with P).

Note that Li migration barriers of both CMP and NMP monolayers are much lower than the commercial anode materials, such as TiO<sub>2</sub> (with Li diffusion barrier of 0.35-0.65 eV<sup>18,65-67</sup>) and silicon ( $\sim 0.57 \text{ eV}^{68}$ ), and are comparable many 2D anode materials, such as  $Mo_2P$  (0.051 eV), <sup>37</sup>  $MoS_2$  (0.25 eV), <sup>69–72</sup>  $Mo_2C$ (0.043 eV),<sup>21</sup> VS<sub>2</sub> (0.22 eV),<sup>17,72</sup> Ti<sub>2</sub>C<sub>3</sub> (0.068 eV),<sup>73</sup> graphene (0.33 eV), 8,74 and black phosphorus (0.084 eV). To get a further impression about the Li mobility on CMP and NMP monolayers, we roughly estimated the relative constant diffusion D at the room temperature by Arrhenius equation (Eqn 4), and found that the D value on the CMP (NMP) monolayer is around twice faster than that on Mo<sub>2</sub>P,<sup>37</sup> and

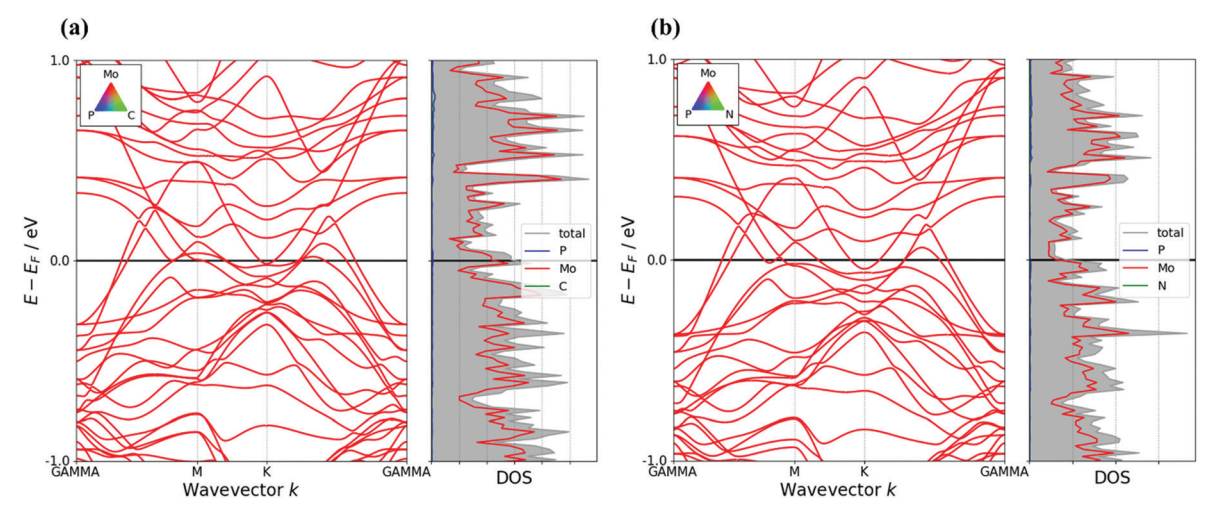


Fig. 2 The electronic band structure and projected densities of states of (a) CMP and (b) NMP monolayers.

(b) (a) S1-S1 S2-S2 S1-S2-S1 S2-S1-S2 € 0.10 S1-S3-S1 S2-S3-S2 ence of diffusion energy 0.06 diffusion 0.04

Fig. 3 (a) Schematic representations of the top view of the migration pathways and the energy profile of diffusion for three pathways S1-S1, S1-S2-S1, and S1-S3-S1 for CMP, (b) schematic representations of the top view of the migration pathways and the energy profile of diffusion for two pathways S2-S2, S2-S1-S2, and S2-S3-S2 for NMP. The pink, blue, grey, and dark blue circles represent P, Mo, C, and N atoms, respectively.

Difference of 6

 $3.7(3.9) \times 10^3$  times faster than that on MoS<sub>2</sub>, <sup>69,70</sup> and 8.3(8.6) × 10<sup>3</sup> times faster than that on graphene.<sup>8,74</sup> Clearly, by simple doping the heteroatoms to Mo<sub>2</sub>P monolayer, the resulting CMP and NMP monolayers have a much accelerated the charging/ discharging capability, which can efficiently improve the cycling and rate performance. To further validate the heteroatoms strategy confirming reducing Li diffusion's energy barrier, we adopt the AIMD simulation method<sup>76–80</sup> to derive the activation energy by using the model that contains one Li atom on CMP. As a result, the activation energy of CMP can be obtained from the Arrhenius plot for the various diffusion coefficients at temperatures from 400 K to 800 (Table S1 and Fig. S8, ESI†). The energy barrier (0.044 eV) is very close to the result (0.037 eV) from the NEB simulation, which will further confirm our NEB result.

Diffusion path (Å)

0.02

#### 3.4. Theoretical voltage profile of lithiation and maximum storage capacity in CMP and NMP

Open-circuit voltage (OCV), the maximum output voltage, is another important parameter to evaluate the performance of the anode materials. The charge/discharging processes of the stable voltage platforms are corresponding to the lithiation/ delithiation reactions of LIBs. Besides, the specific capacity of adsorption anode materials can be obtained when the maximum number of adsorbed Li atoms is known. Here, we systematically examined 10 different Li concentrations (i.e.,  $Li_x$ CMP and  $Li_x$ NMP, x = 1, 2, 3, 4, 6, 8, 9, 18, 27, and 36)(Fig. S9, ESI†).

Our computations showed that all the Li absorption configurations being investigated are stable. The maximum adsorption Li concentration in the lithiated CMP and NMP corresponds to Li<sub>1</sub>Mo<sub>0.50</sub>P<sub>0.222</sub>C<sub>0.028</sub> and Li<sub>1</sub>Mo<sub>0.50</sub>P<sub>0.222</sub>N<sub>0.028</sub>, respectively, which includes 36 Li atoms in a CMP or NMP supercell (containing 27 atoms). In other words, the CMP or MMP monolayer can adsorb two layers of Li atoms on each side of the surface (Fig. S9, ESI†). Similar multilayer adsorption behavior has been observed in TiC<sub>3</sub><sup>81</sup> and TiC<sub>2</sub>O<sub>2</sub>.<sup>82</sup>

Diffusion path (Å)

The doped CMP and NMP anode materials remain metallic after lithiation at different degrees (Fig. 4a and b; and Fig. S10 and S11, ESI†), and the densest TDOS is observed around the Fermi level when the anode surface has the largest coverage, indicating that lots of active electrons are available for high electrical conductivity.

The concentration-dependent adsorption energies  $(E_{ad})$  of Li on CMP and NMP monolayers (Fig. 5a) exhibits the same trend, *i.e.*, its values decrease with increasing the degree of lithiation. Specifically, when only a single Li atom is adsorbed on the surface of CMP, the adsorption energy is ca. -0.62 eV, and the corresponding value on NMP is -0.61 eV. With increasing the degree of lithiation, the  $E_{ad}$  values in  $Li_x$ CMP are both -0.73 eV when x reaches 0.25 and 0.5, and the corresponding values in  $\text{Li}_x$ NMP are -0.76 and -0.77 eV. For the maximum intercalation state x = 1, the  $E_{ad}$  values on CMP and NMP monolayers (-0.38 and -0.40 eV, respectively) remain quite favorable, indicating its possibility for adsorbing more Li atoms, which will not be further considered in this study.

**PCCP** Paper

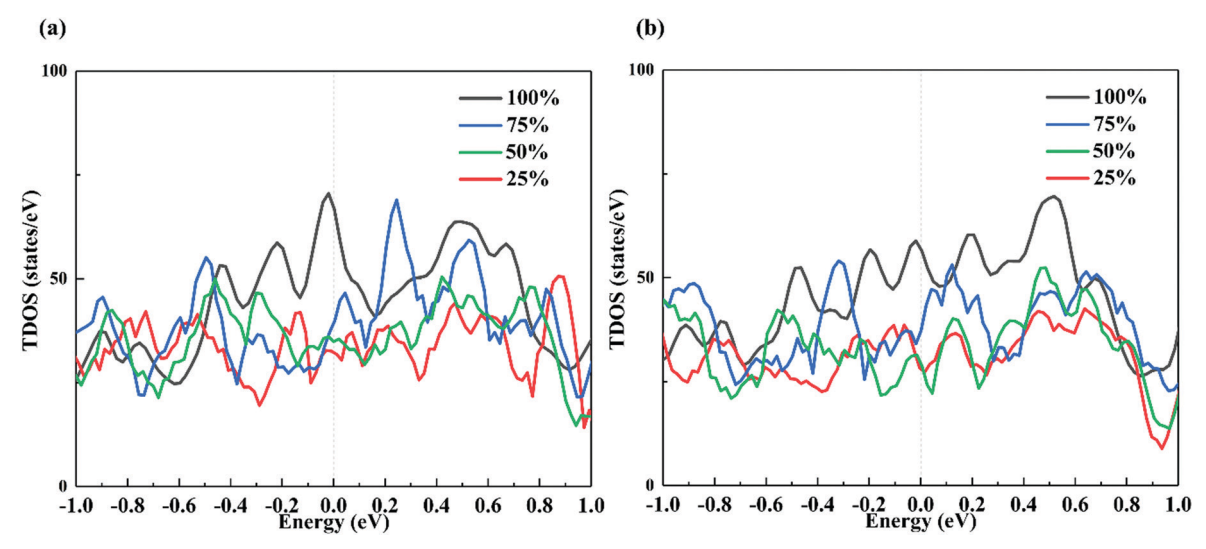


Fig. 4 The total density of states (TDOS) for the (a) CMP and (b) NMP monolayers at various degrees of lithiation. The Fermi level is set to zero

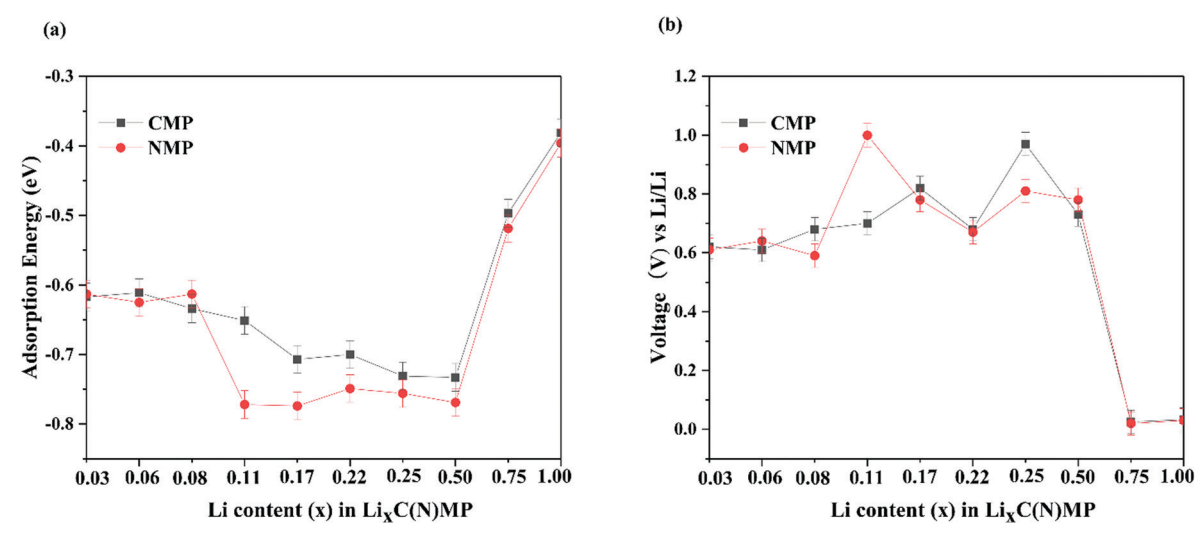


Fig. 5 (a) The variation of adsorption energy with increasing Li contents in CMP and NMP monolayers. (b) OCV as a function of Li content x on the CMP and NMP. The corresponding schematics of Li<sub>x</sub>CMP and Li<sub>x</sub>NMP (top view and side view) are given in Fig. S9 (ESI†).

Typically, the lithiated monolayers anode electrodes do not suffer the metal clustering problems if the adsorption energies are negative numbers.83 For further checking the thermodynamical stability of Li cluster (four atoms cluster), we found that the energy of cluster formation is higher 1.57 eV (2.08 eV) than the same number of Li adatom on the 2D surface of CMP(NMP), which further confirms that the CMP(NMP) are thermodynamically unfavorable to form the Li clusters.

The dopant concentration plays an important role in the capacity and stability of LIBs. To gain insight into the dopant level, we calculated the high doping level of 7.4% for  $Mo_{0.500}P_{0.194}C_{0.056}$  (named as C2MP) and  $Mo_{0.500}P_{0.194}N_{0.056}$ (named as N2MP). The formation energy of C2MP is a positive value of 1.03 eV relatively compared to CMP, suggesting the high C dopant content is unfavorable. It worth noting that the capacity was decreased in high carbon-doped concentration

compared to CMP based on the adsorption energy of Li<sub>1</sub>C2MP is unstable during the optimized process. In N2MP, formation energy is a negative value of -0.32 eV relatively compared to NMP, suggesting the high nitrogen dopant content is thermodynamically stable. Note that the N2MP has potential to increase the capacity because of the high adsorption energy compared to that in NMP (-0.97 eV for  $Li_{0.028}N2MP$ ; -0.81 eV for  $Li_{0.25}N2MP$ ; -0.79 eV for  $Li_{0.5}N2MP$ ; -0.41 eV for Li<sub>1</sub>N2MP.). Overall, the result suggested that the carbondoped Mo<sub>2</sub>P prefers low-level dopant concentration for high capacity, while the nitrogen-doped Mo<sub>2</sub>P prefers high-level dopant concentration for high capacity, which can be the guidance for experimental study.

A high OCV value may contribute to its lithium storage capacity, but hinder the process of charge-discharge. To meet the needs of rapid charge/discharge, the OCV should not be too

high, low OCV and reasonably high OCV values are needed for anode and cathode materials, respectively. For anode materials, typically the desired OCV range is 0.1-1 V, because it can help prevent dendrite formation of alkali metals during the discharge/charge process.21 Herein, we calculated the OCVs profiles of different intercalation states of Li<sub>r</sub>C(N)MP according to eqn (3), and Fig. 5b presents the OCV values as a function of Li content x on the CMP and NMP. In general, the OCV values decrease with increasing lithiation: when only one layer of Li atom is adsorbed on each side of the anode materials (corresponding to x = 0.5), the OCV values are 0.73 and 0.78 V for CMP and NMP, respectively; further lithiation reduces the OCV values, and both CMP and NMP are 0.03 V when those reaches 1.0. Nevertheless, the average OCVs of CMP and NMP are 0.38 V and 0.40 V, respectively, which are comparable to the common commercial anode materials, such as for graphite ( $\sim 0.2 \text{ V}$ ),  $^{8,74}$ and TiO<sub>2</sub> (1.5-1.8 V). 18,65-67 The rather low or moderate OCVs are beneficial for CMP and NMP monolayers to be used as anode materials.

The maximum storage capacity  $(C_{SP})$  is the most critical parameter to evaluate an electrode material. We calculated the specific capacities of CMP and NMP monolayers following eqn (5) using the  $(2 \times 2 \times 1)$  supercell modes using the same method with previous literature. 83,84 The  $C_{\rm SP}$  values increase as Li atoms are gradually added to the anode surface during the lithiation process. Based on the highest lithiation state examined, which corresponds to the chemical formula of  $LiMo_{0.50}P_{0.222}C(N)_{0.028}$ , we determined the theoretical maximum storage capacity capacities of CMP and NMP systems as 485.76 and 485.10 mA h  $g^{-1}$ , respectively. Encouragingly, our estimated maximum storage capacities of CMP and NMP monolayers are larger than many other 2D anode materials, such as Mo<sub>2</sub>P (240 mA h  ${\rm g}^{-1}),^{37} {\rm Mo}_2 {\rm C}$  (400 mA h  ${\rm g}^{-1}),^{21} {\rm VS}_2$  (466 mA h  ${\rm g}^{-1}),^{17} {\rm }$   $\alpha$ -FeSe (340 mA h g<sup>-1</sup>), 85 MXenes (447.8 mA h g<sup>-1</sup>), 73 phosphorene  $(389.02 \text{ mA h g}^{-1})$ ,  $^{75,86}$  and graphite  $(372 \text{ mA h g}^{-1})$ .  $^{8,74}$  The high specific capacities of CMP and NMP monolayers can be attributed to the heteroatom dopants (C and N), which enhance the interactions between the intercalation host and the lithium atoms.

The thermal stability is another important descriptor for anode materials, which can be estimated at different temperatures by MD simulations. It complements the thermodynamic and dynamic stabilities evaluated by the formation energies and phonon dispersion curves at absolute zero temperature. Thus, we conducted extensive AMID simulations for CNP and NMP monolayers adsorbed by one-layer Li atoms at each side of the surface (Li<sub>0.5</sub>CMP and Li<sub>0.5</sub>NMP, corresponding to the chemical formulas of  $\mathrm{Li}_{0.5} Mo_{0.50} P_{0.222} C_{0.028}$  and  $\text{Li}_{0.5}\text{Mo}_{0.50}\text{P}_{0.222}\text{N}_{0.028}\text{, respectively})$  at different temperatures. All the structures along the trajectory are recorded for Li<sub>0.5</sub>CMP (Fig. S12a and Movie S7, ESI†) and Li<sub>0.5</sub>NMP (Fig. S12b and Movie S8, ESI†). Both Li<sub>0.5</sub>CMP and Li<sub>0.5</sub>NMP do not collapse throughout the 10 ps AIMD simulation at room temperature. Considering that the temperature of LIBs would increase during the charge/discharge process, we performed further AIMD simulations at higher temperatures and found that the Li<sub>0.5</sub>CMP and Li<sub>0.5</sub>NMP structures are not disrupted up to 500 K

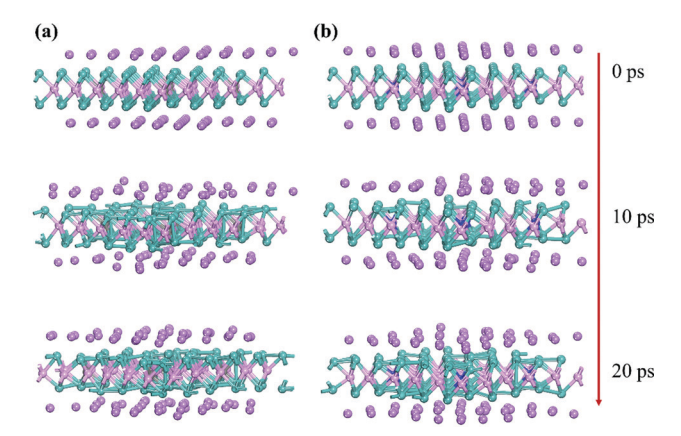


Fig. 6 Snapshots of structures of (a) the CMP monolayers and (b) the NMP monolayers following a 20 ps AIMD simulation at 500 K. The pink, blue, grey, and navy atoms represent P, Mo, C, and N atoms, respectively.

during a simulation time of 20 ps (Fig. 6a and b). Thus, both CMP and NMP are expected to have good thermal stability.

## 4. Conclusion

In summary, by systematic DFT computations and ab initio molecular dynamics simulations, we explored the potential to improve the performance of Mo<sub>2</sub>P monolayer as LIB anode materials by simple doping C and N heteroatoms. Compared with the pristine Mo<sub>2</sub>P monolayer, the resulting C- and N-doped Mo<sub>2</sub>P (CMP and NMP) monolayers have a lower Li diffusion barrier (~0.036 eV) along the 2D plane, and can double the specific capacity (485.76 and 485.10 mA h  $g^{-1}$ , respectively). The average OCVs of Li intercalation for CMP and NMP (0.38 and 0.40 eV, respectively) are in a good range (0.1-1 V) for LIB anodes. After lithiation, both CMP and NMP monolayers can remain stable at a high temperature (up to 500 K) and preserve the intrinsic metallic character. All these computations demonstrated that the simple doing with wisely chosen heteroatoms serves as an effective method to improve the performance of 2D TMPs as electrode materials.

#### Conflicts of interest

The authors declare no competing interests.

## Acknowledgements

This work was financially supported in Korea by the Institute for Basic Science (IBS-R011-D1), and in USA by NASA (Grant Number 80NSSC19M0236) and NSF Center for the Advancement of Wearable Technologies (Grant 1849243). SGK's work was supported by the Creative Materials Discovery Program through the National Research Foundation of Korea (NRF) funded by the Ministry of Science, ICT, and Future Planning (No. 2016M3D1A1919181). We thank Jinxing Gu (Department of Chemistry University of Puerto Rico) and Ziheng Lu (Department

of Materials Science & Metallurgy University of Cambridge) for the useful discussion.

## References

- 1 D. P. Dubal, O. Ayyad, V. Ruiz and P. Gomez-Romero, Chem. Soc. Rev., 2015, 44, 1777-1790.
- 2 J. W. Choi and D. Aurbach, Nat. Rev. Mater., 2016, 1, 1-16.
- 3 M. Li, J. Lu, Z. Chen and K. Amine, Adv. Mater., 2018, 30, e1800561.
- 4 M. S. Dresselhaus and I. L. Thomas, Nature, 2001, 414, 332-337.
- 5 V. Etacheri, R. Marom, R. Elazari, G. Salitra and D. Aurbach, Energy Environ. Sci., 2011, 4, 3243-3262.
- 6 M. Y. Li, Y. Shi, C. C. Cheng, L. S. Lu, Y. C. Lin, H. L. Tang, M. L. Tsai, C. W. Chu, K. H. Wei, J. H. He, W. H. Chang, K. Suenaga and L. J. Li, Science, 2015, 349, 524-528.
- 7 M. Acerce, D. Voiry and M. Chhowalla, Nat. Nanotechnol., 2015, 10, 313-318.
- 8 Y. Jing, Z. Zhou, C. R. Cabrera and Z. F. Chen, J. Mater. Chem. A, 2014, 2, 12104-12122.
- 9 L. L. Peng, Y. Zhu, D. H. Chen, R. S. Ruoff and G. H. Yu, Adv. Energy Mater., 2016, 6, 1600025.
- 10 H. Cui, Y. Guo, W. Ma and Z. Zhou, ChemSusChem, 2020, 13, 1155-1171.
- 11 C. Zhu, S. Lin, M. Zhang, Q. Li, Z.-M. Su and Z. Chen, J. Mater. Chem. A, 2020, 8, 10301-10309.
- 12 Q. Tang, Z. Zhou and Z. Chen, Nanoscale, 2013, 5, 4541-4583.
- 13 Y. Jing, E. O. Ortiz-Quiles, C. R. Cabrera, Z. F. Chen and Z. Zhou, Electrochim. Acta, 2014, 147, 392-400.
- 14 K. Persson, Y. Hinuma, Y. S. Meng, A. Van der Ven and G. Ceder, Phys. Rev. B: Condens. Matter Mater. Phys., 2010, 82, 125416.
- 15 K. Tu, F. Li and Z. Chen, J. Mater. Res., 2015, 31, 878-885.
- 16 E. Yang, H. Ji and Y. Jung, J. Phys. Chem. C, 2015, 119, 26374-26380.
- 17 Y. Jing, Z. Zhou, C. R. Cabrera and Z. F. Chen, J. Phys. Chem. C, 2013, 117, 25409-25413.
- 18 M. V. Koudriachova, N. M. Harrison and S. W. de Leeuw, Solid State Ionics, 2002, 152, 189-194.
- 19 C. Eames and M. S. Islam, J. Am. Chem. Soc., 2014, 136, 16270-16276.
- 20 J. J. Zhu, A. Chroneos and U. Schwingenschlogl, Phys. Status Solidi RRL, 2015, 9, 726-729.
- 21 D. Çakır, C. Sevik, O. Gülseren and F. M. Peeters, J. Mater. Chem. A, 2016, 4, 6029-6035.
- 22 Q. Tang, Z. Zhou and P. Shen, J. Am. Chem. Soc., 2012, 134, 16909-16916.
- 23 H. G. Von Schnering and W. Hönle, Chem. Rev., 1988, 88,
- 24 Y. Shi and B. Zhang, Chem. Soc. Rev., 2016, 45, 1529-1541.
- 25 Y. Pei, Y. Cheng, J. Chen, W. Smith, P. Dong, P. M. Ajayan, M. Ye and J. Shen, J. Mater. Chem. A, 2018, 6, 23220-23243.
- 26 S. T. Oyama, T. Gott, H. Y. Zhao and Y. K. Lee, Catal. Today, 2009, 143, 94-107.

- 27 S. T. Oyama, J. Catal., 2003, 216, 343-352.
- 28 V. Pralong, D. Souza, K. Leung and L. Nazar, Electrochem. Commun., 2002, 4, 516-520.
- 29 S. Carenco, D. Portehault, C. Boissiere, N. Mezailles and C. Sanchez, Chem. Rev., 2013, 113, 7981-8065.
- 30 Z. Q. Liang, R. J. Huo, S. H. Yin, F. Z. Zhang and S. L. Xu, J. Mater. Chem. A, 2014, 2, 921-925.
- 31 S. Boyanov, K. Annou, C. Villevieille, M. Pelosi, D. Zitoun and L. Monconduit, Ionics, 2008, 14, 183-190.
- 32 J. Cabana, L. Monconduit, D. Larcher and M. R. Palacin, Adv. Mater., 2010, 22, E170-E192.
- 33 J. Yin, B. Wu, Y. Wang, Z. Li, Y. Yao, Y. Jiang, Y. Ding, F. Xu and P. Zhang, J. Phys.: Condens. Matter, 2018, 30, 135701.
- 34 W. Ming, M. Yoon, M. H. Du, K. Lee and S. W. Kim, J. Am. Chem. Soc., 2016, 138, 15336-15344.
- 35 Y. F. Shao, X. Q. Shi and H. Pan, Chem. Mater., 2017, 29, 8892-8900.
- 36 S. Yang, G. Chen, A. G. Ricciardulli, P. Zhang, Z. Zhang, H. Shi, J. Ma, J. Zhang, P. W. M. Blom and X. Feng, Angew. Chem., Int. Ed., 2020, 59, 465-470.
- 37 B. Mortazavi, M. Shahrokhi, M. Makaremi and T. Rabczuk, Appl. Mater. Today, 2017, 9, 292-299.
- 38 D. Wu, S. Wang, S. Zhang, Y. Liu, Y. Ding, B. Yang and H. Chen, Phys. Chem. Chem. Phys., 2019, 21, 1029-1037.
- 39 Y. Li, D. Wu, Z. Zhou, C. R. Cabrera and Z. Chen, J. Phys. Chem. Lett., 2012, 3, 2221-2227.
- 40 M. Yang, Y. R. Zhong, J. J. Ren, X. L. Zhou, J. P. Wei and Z. Zhou, Adv. Energy Mater., 2015, 5, 1500550.
- 41 J. Q. Yang, X. L. Zhou, D. H. Wu, X. D. Zhao and Z. Zhou, Adv. Mater., 2017, 29, 1604108.
- 42 H. J. Cui, Z. Zhou and D. Z. Jia, Mater. Horiz., 2017, 4, 7-19.
- 43 A. L. Reddy, A. Srivastava, S. R. Gowda, H. Gullapalli, M. Dubey and P. M. Ajayan, ACS Nano, 2010, 4, 6337–6342.
- 44 J. X. Song, T. Xu, M. L. Gordin, P. Y. Zhu, D. P. Lv, Y. B. Jiang, Y. S. Chen, Y. H. Duan and D. H. Wang, Adv. Funct. Mater., 2014, 24, 1243-1250.
- 45 C. C. Ma, X. H. Shao and D. P. Cao, J. Mater. Chem., 2012, 22, 8911-8915.
- 46 X. H. Liu, J. Zhang, S. J. Guo and N. Pinna, J. Mater. Chem. A, 2016, 4, 1423-1431.
- 47 S. Z. Huang, Y. Li, Y. Y. Feng, H. R. An, P. Long, C. Q. Qin and W. Feng, J. Mater. Chem. A, 2015, 3, 23095-23105.
- 48 G. Kresse and J. Hafner, Phys. Rev. B: Condens. Matter Mater. Phys., 1994, 49, 14251-14269.
- 49 G. Kresse and J. Hafner, Phys. Rev. B: Condens. Matter Mater. Phys., 1993, 47, 558-561.
- 50 G. Kresse and J. Furthmuller, Phys. Rev. B: Condens. Matter Mater. Phys., 1996, 54, 11169-11186.
- 51 P. E. Blochl, Phys. Rev. B: Condens. Matter Mater. Phys., 1994, 50, 17953-17979.
- 52 G. Kresse and D. Joubert, Phys. Rev. B: Condens. Matter Mater. Phys., 1999, 59, 1758-1775.
- 53 J. P. Perdew, K. Burke and M. Ernzerhof, Phys. Rev. Lett., 1996, 77, 3865-3868.
- 54 H. J. Monkhorst and J. D. Pack, Phys. Rev. B: Solid State, 1976, 13, 5188-5192.

55 A. Togo, F. Oba and I. Tanaka, *Phys. Rev. B: Condens. Matter Mater. Phys.*, 2008, **78**, 134106.

- 56 G. J. Martyna, M. L. Klein and M. Tuckerman, *J. Chem. Phys.*, 1992, **97**, 2635–2643.
- 57 S. Grimme, J. Antony, S. Ehrlich and H. Krieg, *J. Chem. Phys.*, 2010, **132**, 154104.
- 58 G. Henkelman, B. P. Uberuaga and H. Jonsson, *J. Chem. Phys.*, 2000, **113**, 9901–9904.
- 59 G. Henkelman and H. Jonsson, *J. Chem. Phys.*, 2000, **113**, 9978–9985.
- 60 A. Savin, R. Nesper, S. Wengert and T. F. Fässler, *Angew. Chem., Int. Ed. Engl.*, 1997, **36**, 1808–1832.
- 61 R. F. Bader, Acc. Chem. Res., 1985, 18, 9-15.
- 62 H. Yildirim and R. Pachter, ACS Appl. Electron. Mater., 2019, 1, 467–477.
- 63 V. Q. Bui, A. Kumar, H. T. Bui, J. Lee, Y. Hwang, H. M. Le, Y. Kawazoe and H. Lee, *Chem. Mater.*, 2020, 32(22), 9591–9601.
- 64 M. Jäckle and A. Groß, J. Chem. Phys., 2014, 141, 174710.
- S. Lunell, A. Stashans, L. Ojamae, H. Lindstrom and A. Hagfeldt, J. Am. Chem. Soc., 1997, 119, 7374–7380.
- 66 H. Lindström, S. Södergren, A. Solbrand, H. Rensmo, J. Hjelm, A. Hagfeldt and S.-E. Lindquist, *J. Phys. Chem. B*, 1997, **101**, 7710–7716.
- 67 C. L. Olson, J. Nelson and M. S. Islam, J. Phys. Chem. B, 2006, 110, 9995–10001.
- 68 Z. Wang, Q. Su, H. Deng, W. He, J. Lin and Y. Q. Fu, J. Mater. Chem. A, 2014, 2, 13976–13982.
- 69 H. Hwang, H. Kim and J. Cho, *Nano Lett.*, 2011, **11**, 4826–4830.
- 70 S. Ding, D. Zhang, J. S. Chen and X. W. Lou, *Nanoscale*, 2012, 4, 95–98.

- 71 Y. Li, D. Wu, Z. Zhou, C. R. Cabrera and Z. Chen, *J. Phys. Chem. Lett.*, 2012, 3, 2221–2227.
- 72 Y. Jing, Z. Zhou, C. R. Cabrera and Z. Chen, *J. Phys. Chem. C*, 2013, **117**, 25409–25413.
- 73 D. Q. Er, J. W. Li, M. Naguib, Y. Gogotsi and V. B. Shenoy, *ACS Appl. Mater. Interfaces*, 2014, **6**, 11173–11179.
- 74 C. Uthaisar and V. Barone, Nano Lett., 2010, 10, 2838-2842.
- 75 W. Li, Y. Yang, G. Zhang and Y. W. Zhang, *Nano Lett.*, 2015, 15, 1691–1697.
- 76 Y. Mo, S. P. Ong and G. Ceder, *Chem. Mater.*, 2012, 24, 15–17.
- 77 Z. Lu, J. Liu and F. Ciucci, Energy Storage Mater., 2020, 28, 146–152.
- 78 Z. Deng, Y. Mo and S. P. Ong, NPG Asia Mater., 2016, 8, e254.
- 79 V. Wang, N. Xu, J. C. Liu, G. Tang and W.-T. Geng, 2019, arXiv preprint arXiv:1908.08269.
- 80 Z. Lu, F. Sui, Y.-E. Miao, G. Liu, C. Li, W. Dong, J. Cui, T. Liu, J. Wu and C. Yang, J. Energy Chem., 2020, 58, 170–198.
- 81 Y. Xie, M. Naguib, V. N. Mochalin, M. W. Barsoum, Y. Gogotsi, X. Yu, K.-W. Nam, X.-Q. Yang, A. I. Kolesnikov and P. R. Kent, *J. Am. Chem. Soc.*, 2014, 136, 6385–6394.
- 82 T. Yu, Z. Zhao, L. Liu, S. Zhang, H. Xu and G. Yang, *J. Am. Chem. Soc.*, 2018, **140**, 5962–5968.
- 83 C. Zhu, S. Lin, M. Zhang, Q. Li, Z. Su and Z. Chen, *J. Mater. Chem. A*, 2020, **8**, 10301–10309.
- 84 S. Ullah, P. A. Denis and F. Sato, *Appl. Mater. Today*, 2017, 9, 333–340.
- 85 D. Wei, J. Liang, Y. Zhu, L. Hu, K. Zhang, J. Zhang, Z. Yuan and Y. Qian, *Electrochem. Commun.*, 2014, 38, 124–127.
- 86 A. Sibari, A. El Marjaoui, M. Lakhal, Z. Kerrami, A. Kara, M. Benaissa, A. Ennaoui, M. Hamedoun, A. Benyoussef and O. Mounkachi, Sol. Energy Mater. Sol. Cells, 2018, 180, 253–257.